# DEVELOPMENT OF THE TRAPPE FORCE FIELD FOR AMMONIA

Ling ZHANG and J. Ilja SIEPMANN[1,*]

*Departments of Chemistry and of Chemical Engineering and Materials Science, University of Minnesota, 207 Pleasant St. SE, Minneapolis, MN 55455-0431, USA; e-mail: [1] siepmann@umn.edu*

Received November 2, 2009
Accepted February 17, 2010
Published online May 20, 2010

*Dedicated to Professor Ivo Nezbeda on the occasion of his 65th birthday.*

The transferable potentials for phase equilibria (TraPPE) force field is extended through the development of a non-polarizable five-site ammonia model. In this model, the electrostatic interactions are represented by three positive partial charges placed at the hydrogen position and a compensating partial charge placed on an M site that is located on the $C_3$ molecular axis and displaced from the nitrogen atom toward the hydrogen atoms. The repulsive and dispersive interactions are represented by placing a single Lennard–Jones site at the position of the nitrogen atom. Starting from the five-site model by Impey and Klein (*Chem. Phys. Lett.* **1984**, *104*, 579), this work optimizes the Lennard–Jones parameters and the magnitude of the partial charges for three values of the M site displacement. This parameterization is done by fitting to the vapor–liquid coexistence curve of neat ammonia. The accuracy of the three resulting models (differing in the displacement of the M site) is assessed through computation of the binary vapor–liquid equilibria with methane, the structure and the dielectric constant of liquid ammonia. The five-site model with an intermediate displacement of 0.08 Å for the M site yields a much better value for the dielectric constant, whereas differences in the other properties are quite small.

**Keywords**: Ammonia; Monte Carlo simulation; Transferable force field; Vapor–liquid equilibrium.

Ammonia is not only an important chemical intermediate, but also an example of a small molecule that can self-associate via hydrogen bonding. Thus, ammonia has been the topic of numerous experimental, theoretical, and molecular simulation studies. When molecular simulation is utilized to predict the thermophysical properties of a specific chemical system, then its success relies on the availability of accurate molecular models, whereas simpler models are more appropriate to delineate the phenomenological



doi:10.1135/cccc2009540

properties of a class of compounds. Many excellent examples of the latter class of models have been proposed by Nezbeda and co-workers[1–5].

The first specific molecular models for ammonia were developed in the 1980s. Initially, Jorgensen and Ibrahim[6] and Hinchliffe et al.[7] developed four-site models to reproduce sets of dimer energies determined from electronic structure calculations. Both of these models made use of experimental information to set the N–H bond length and H–N–H angle and placed four partial charges on the atomic sites and one repulsive-dispersive site on the position of the nitrogen atom. In 1984, Impey and Klein[8] constructed a rigid five-site ammonia model with one Lennard–Jones site placed at the nitrogen position, three charge sites placed at the hydrogen positions and one additional charge site, called M site, located on the $C_3$ molecular axis, 0.156 Å toward the hydrogen atoms. The N–H bond length and the H–N–H bend angle of the Impey–Klein model were chosen in accordance with experimental data[9], and the Lennard–Jones parameters and the location of the M site were optimized to reproduce the N–N radial distribution function determined by Narten[10]. All of these early models use a rigid geometry, but a flexible four-site model has also been proposed by Rizzo and Jorgensen[11] with the nonbonded parameters primarily fitted to the experimental liquid density and heat of vaporization at 240 K and 1 atm; hydrogen bond energetics with water and the free energy of hydration relative to methylamine were also taken into consideration for further parameterization.

Although these early models have been used to study many different aspects of liquid ammonia, their capability for predicting accurate vapor–liquid coexistence curves had not been assessed until more recently. In 1999, Kristof et al.[12] explored both four- and five-site ammonia models, the latter with an N–M distance of 0.1907 Å close to the geometry used by Impey and Klein[8]. The vapor–liquid coexistence curves for both models developed by Kristof et al. show great improvement in reproducing the experimental vapor–liquid coexistence curve compared to Impey and Klein's model. The pair distribution functions in the liquid state predicted by these models are also in fairly good agreement with experimental X-ray and neutron diffraction results. Although the four-site model recommended by Kristof et al. satisfactorily reproduces the vapor pressure and critical temperature, the critical density is 5% too low, and the dielectric constant of liquid phase is found to be 50% too high.

Prompted by this disagreement, we have explored whether a five-site model with a different displacement for the M site might yield improved results[13]. In this study, the complexity of the ammonia model follows that of the Impey and Klein model, i.e., the model uses a rigid geometry, a fixed set

of partial charges, and only a single Lennard–Jones site to account for the repulsive–dispersive interactions. Three different choices of the N–M distance were investigated and for each choice the three nonbonded parameters were fitted to the vapor–liquid coexistence curve of neat ammonia. Such a parameterization approach is sufficient for many molecules, particularly for non-polar molecules[14–20] or for polar molecules when some of the parameters can be transfered from other molecules[21–25]. However, it was previously noted that fitting to the vapor–liquid coexistence curve of the neat compound is not sufficient when the compound is not a part of a homologous series and both Lennard–Jones and partial charges need to be determined from scratch. In these cases, additional data such as binary vapor–liquid equilibria[26] or solid–fluid equilibria[27] can be used to empirically optimize the parameters. Indeed, it is also found here that multiple parameter sets for ammonia perform nearly equally well, and additional optimization criteria, such as the binary vapor–liquid equilibrium of ammonia–methane mixture and the dielectric constant of liquid ammonia are considered for the determination of the final selection. It should also be noted that Eckl et al.[28] have recently developed a four-site model by optimizing only the two Lennard–Jones parameters and using a geometry and charge distribution obtained from electronic structure calculations; this model significantly outperforms the four-site model by Kristof et al.

## SIMULATION METHODS

The development of the TraPPE model started with the geometric parameters of the Impey and Klein model[8] for the atomic positions, i.e., the N–H bond length is set to 1.0124 Å and the H–N–H bend angle is 106.68°. Given the divergent findings on the necessity of a separate M-site (i.e., four-site versus five-site representation)[8,12], the current work explored three values for the displacement of the M site located on the $C_3$ molecular axis toward the hydrogen atoms: 0.0, 0.08, and 0.16 Å leading to models called here M-0, M-8, and M-16, respectively. The first corresponds to a four-site model, the third is close to the parameter found by Impey and Klein[8], and the other value is an intermediate choice. A single Lennard–Jones site is placed at the position of the nitrogen atom to represent the dispersive and repulsive interactions, and partial charges at the three hydrogen atoms and the M site are used to represent the first-order and induced polarization contributions of the electrostatic energy[29]. This description of the intermolecular interactions results in three adjustable parameters: the partial charge for a hydrogen atom ($q_H = -q_M/3$), the Lennard–Jones diameter ($\sigma$)

and well depth (ε) for the nitrogen atom. It should be noted here that the increase in the computational cost of the energy (force) calculation is minimal when changing from a 4-site model to a (4+1)-site model (4 partial charges + 1 Lennard–Jones site) because the number of distance evaluations increases only from 16 to 17 for a pair of molecules and the cost of the computation of the long-range electrostatic component does not change. In contrast, the 5-site model investigated by Kristof et al.[12] contains 5 partial charges and, hence, 25 site–site distances need to be computed.

For each of the three M site locations, the three nonbonded interaction parameters were optimized by fitting to the vapor–liquid coexistence curve using a stepwise mesh approach. That is, suitable lower and upper bounds for each parameter are deduced from previous ammonia models and experience. This parameter space is then covered by a $4^3$ mesh with even spacing. Relatively short simulations are then performed for each of the mesh points to find the region of parameter space (here, one or two cubes) that yields the best results for a fitness function (see below). This region of parameter space is then again divided into a similar mesh and another set of somewhat longer simulations is performed to locate a smaller region of improved fitness. This may be followed by another iteration with finer mesh and longer simulations. Usually, a total of three or four of these iterations is sufficient to find a set of parameters that satisfies a the fitness function within an acceptable tolerance. The advantages of this stepwise mesh approach are that is very well suited for a massively parallel implementation and not likely to get trapped in local minima in parameter space, but the total computer time required is in many cases larger than for optimization schemes that employ a series expansion around an initial parameter set[20,28].

In the development of the TraPPE force field the fitness function is the sum of the mean unsigned percentage errors for the critical temperature, the normal boiling point, the saturated liquid density, and the saturated vapor pressure (usually weighted with a prefactor of 0.1 to account for the larger uncertainties in this property) where the latter two properties are averaged over multiple temperatures and only these average errors enter into the fitness function. The initial parameter ranges and the optimized parameters of the three models (M-0, M-8, and M-16) are listed together with the parameters of previous models in Table I. It should be noted here that the optimized charges for model M-0 are identical to those found by Kristof et al.[12] for their four-site model, while the Lennard–Jones well depth of models M-0 and M-8 is close to that of the optimized model by Eckl et al.[28]. As one might expect, the mesh data also indicate that increasing the N–M

distance without adjusting the $q_H$ and Lennard–Jones parameters results in a downward shift of the vapor–liquid coexistence curve due to the decrease in the dipole moment and, hence, reduction of the first-order electrostatic interactions.

Due to the rigid nature of the ammonia model (and also of the TraPPE-EH methane model[16]), the potential energy of the simulated systems includes only the intermolecular pairwise-additive Lennard–Jones and Coulombic terms (the latter using the permittivity of the vacuum). The Lennard–Jones parameters for unlike pairs (the methane model consists of Lennard–Jones sites on the carbon atom and the C–H bond centers) are determined from the standard Lorentz–Berthelot combining rules[29]. The simulations employed a spherical potential cutoff, $r_{cut}$ = 14 Å, and analytic tail corrections for the Lennard–Jones interactions[30,31]. The Coulombic interactions were computed using the Ewald summation technique with tin foil boundary conditions[31] with the real-space cutoff set equal to $r_{cut}$ and the Ewald sum convergence parameter set to $3.5/r_{cut}$. Finally, to avoid unphysically strong interactions of the unprotected polar hydrogen atoms

TABLE I
Comparison of nonbonded parameters for ammonia models

| Parameter range | $d_{N-M}$, Å | $\varepsilon/k_B$, K | σ, Å | $q_H$, e |
|---|---|---|---|---|
| | 0.0 | 150–215 | 3.36–3.40 | 0.33–0.36 |
| | 0.08 | 150–205 | 3.36–3.42 | 0.37–0.45 |
| | 0.16 | 150–220 | 3.36–3.45 | 0.42–0.50 |
| Optimized models | $d_{N-M}$, Å | $\varepsilon/k_B$, K | σ, Å | $q_H$, e |
| M-0 | 0.0 | 180 | 3.40 | 0.345 |
| M-8 | 0.08 | 185 | 3.42 | 0.41 |
| M-16 | 0.16 | 210 | 3.41 | 0.46 |
| Other models | $d_{N-M}$, Å | $\varepsilon/k_B$, K | σ, Å | $q_H$, e |
| Impey and Klein[8] | 0.156 | 140 | 3.40 | 0.462 |
| Kristof et al.[12] | 0.0 | 170 | 3.385 | 0.345 |
| Eckl et al.[28] | 0.0 | 182.9 | 3.376 | 0.3331 |

with the unprotected M site (neither carries a repulsive potential term) or the charged nitrogen site (for model M-0), a minimum separation of 1.0 Å was also enforced between any two sites (i.e., the corresponding hard-sphere potential is added to all site-site interactions). Models using a single Lennard–Jones site on or near the heavy atom but multiple displaced charges on the hydrogen atoms or other positions (additional examples are the well-known SPC, SPC/E, TIP3P, and TIP4P water models) exhibit the severe problem that the minimum dimer configuration with an energy of $-\infty$ is one where the hydrogen atom of molecule A coincides with the nitrogen (or oxygen) atom of molecule B. Although there exists a large energy barrier that separates the physically relevant hydrogen-bonded structure from this unphysical minimum, an efficient Monte Carlo algorithm such as the one used here has no trouble finding the unphysical minimum. The hard-sphere potential removes the unphysical minimum energy structure but does not affect any physically relevant structures.

The canonical (constant-*NVT*) and isothermal-isobaric (constant-*NpT*) versions of the Gibbs ensemble[32,33] were used for simulations of the saturated vapor–liquid coexistence curves for neat ammonia and the binary ammonia–methane mixture, respectively. For the canonical Gibbs ensemble simulation, a system size of 500 ammonia molecules (with the exception of the highest temperature where 1000 molecules were used) was selected to ensure that the linear dimension of the liquid phase is larger than $2r_{cut}$ with the total volume adjusted to result in a vapor phase containing at least 20 molecules. Phase space was sampled through rigid-body translations and rotations, volume exchanges between the two boxes, and particle transfers using the configurational-bias Monte Carlo methodology[34–37]. Simulations were carried at six different temperatures: 200, 250, 300, 350, 375, and 390 K. The simulation lengths varied throughout the parameter optimization, but the production periods for the optimized models consisted of $10^6$ Monte Carlo cycles, where one cycle consists of 500 (or 1000) randomly selected attempted moves.

The critical temperatures ($T_c$) and critical densities ($\rho_c$) were estimated using the saturated density scaling law[38] and the law of rectilinear diameters[39] with a universal scaling exponent[40] of $\beta^* = 0.325$. The critical pressure ($P_c$) was estimated from a fit of the high-temperature saturated vapor pressures to the Antoine equation[41], and the normal boiling point ($T_b$) was determined via a fit of the low-temperature saturated vapor pressures to the Clausius–Clapeyron equation[42].

The system used for the *NpT* Gibbs ensemble simulations of the binary vapor–liquid coexistence curve consisted of 500 ammonia and 500 TraPPE-

EH methane[16] molecules. Simulations were carried out at $T$ = 273.15 K and $p$ = 50, 100, 150, and 200 atm. At least $10^5$ and $10^6$ Monte Carlo cycles were used for equilibration and production, respectively. The initial configuration consisted of neat ammonia and neat methane phases. Each phase was first allowed to equilibrate with the external pressure bath to achieve the correct density under the corresponding temperature and pressure condition; particle swap moves for both types of molecules were then turned on to equilibrate the chemical potentials between the phases.

In addition to the calculations of the vapor–liquid equilibrium properties, single-phase Monte Carlo simulations were carried out to compute the dielectric constant of liquid ammonia, thereby allowing for a further evaluation of the optimized models. The simulations used systems consisting of 500 ammonia molecules. For each model, a long simulation in the isobaric-isothermal ensemble[43] was used to determine the liquid density at $T$ = 239.8 K and $P$ = 1 atm (the experimental normal boiling point). This was followed by a long simulation ($2 \times 10^6$ Monte Carlo cycles) in the canonical ensemble[30] at the equilibrium density. The dielectric constant was computed from the fluctuation of the total system dipole moment, $M$ [31]. The running averages of both $\langle M^2 \rangle - \langle M \rangle^2$ and $\langle M^2 \rangle$ were monitored constantly during the simulation. After both variables converged, the final result of the dielectric constant was computed[44].

## RESULTS AND DISCUSSIONS

The pure component saturated vapor–liquid coexistence curves for the ammonia models are shown in Fig. 1. All three models developed here and the four-site models by Kristof et al.[12] and Eckl et al.[28] reproduce the saturated liquid densities up to 375 K extremely well. Kristof et al.[8] and Eckl et al.[28] also carried out simulations near 385 and 395 K and found slight underestimations of the saturated liquid densities. These deviations are also reflected in slight underestimations of the critical temperature and densities (Table II), whereas the three models developed here very slightly overestimate the critical temperature (by about 0.3%, but within the statistical uncertainty) and the critical density are overestimated by 1.7, 0.9, and 3.8% for models M-0, M-8, and M-16. Model M-0 yields a slightly higher critical temperature than the Kristof et al.[8] and Eckl et al.[28] models because its ε value is higher (stronger dispersive interactions) than that for the Kristof model and its $q_H$ value is higher (stronger first-order electrostatic interactions) than that for the Eckl model (see Table I).

The saturated vapor pressure lines for the different ammonia models are shown in the form of a Clausius–Clapeyron plot in Fig. 2. Again, the performance of the models by Kristof et al.[12], Eckl et al.[28], and of the three models developed here is quite impressive over most of the vapor–liquid re-

TABLE II
Comparison of the critical properties, boiling point, and liquid-phase dielectric constant (at 239.8 K) for different ammonia models. Subscripts denote the uncertainty in the last digit(s)

| Model | $T_c$, K | $r_c$, g cm$^{-3}$ | $P_c$, MPa | $T_b$, K | $\varepsilon_D$ | μ, D |
|---|---|---|---|---|---|---|
| M-0 | $406_2$ | $0.239_3$ | $11.7_5$ | $242_1$ | $37_4$ | 1.90 |
| M-8 | $406_2$ | $0.233_4$ | $11.1_4$ | $241_1$ | $22_2$ | 1.78 |
| M-16 | $407_2$ | $0.244_4$ | $13.5_6$ | $240_1$ | $12_1$ | 1.47 |
| Kristof et al.[12] | 401.7 | 0.224 | 11.2 | – | $35_{10}$ | 1.90 |
| Eckl et al.[28] | 402.2 | 0.228 | 10.5 | 237 | – | 1.94 |
| Experiment[46,47] | 405.7 | 0.235 | 11.3 | 239.8 | 22.4 | 1.47 |

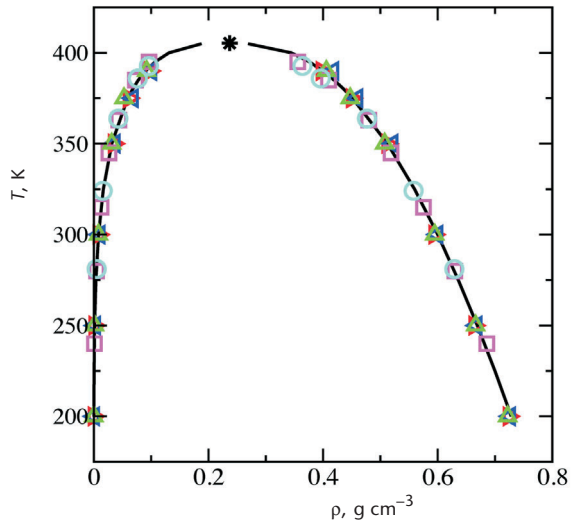


FIG. 1
Comparison of the vapor–liquid coexistence curves predicted by different ammonia models: M-0 (red right triangles), M-8 (green up triangles), M-16 (blue left triangles), Kristof et al.[12] (cyan circles), and Eckl et al.[28] (magenta squares). The experimental coexistence densities[45] and critical point[46] are shown as solid lines and star, respectively. Statistical uncertainties are smaller than the symbol size

gion. Model M-16 slightly overestimates the saturated vapor pressure and the deviations become higher as temperature increases, resulting in an overestimation of the critical pressure by 20%. Model M-8 yields the best agreement with experiment (with the data at 200 K being the exception). The critical pressure and normal boiling point predicted with this model show excellent agreement (deviations of 2 and 0.5%, respectively), whereas model M-0 yields both an overestimation of the critical pressure (by 4%) and of the normal boiling point (by 1%), i.e., the slope of the Clausius–Clapeyron line is too large in magnitude for this model. At elevated temperatures, the model of Kristof et al. yields excellent vapor pressures, but simulation data[12] are not available at temperatures close to the normal boiling point. The model by Eckl et al.[28] appears to overpredict the saturated vapor pressures at low temperatures (by about 20% at 240 K) and, hence, the normal boiling point is underestimated by about 3 K.

Overall, model M-8 and the Eckl et al.[28] model yield slightly better predictions of the neat vapor–liquid equilibrium properties than the Kristof et al.[12], M-0, and M-16 models.

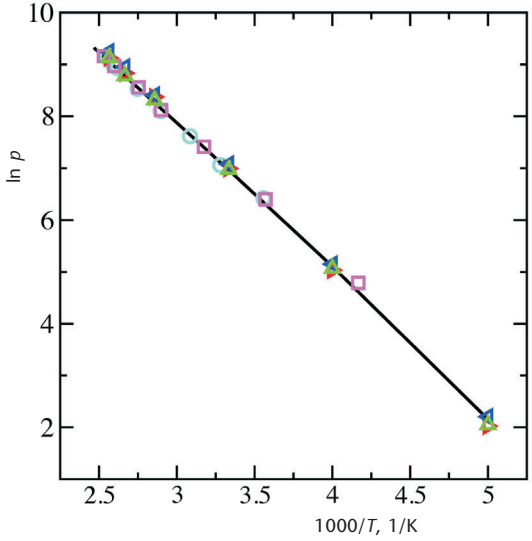


FIG. 2
Comparison of the saturated vapor pressure ($p$ in kPa) lines predicted by different ammonia models. Symbols as in Fig. 1. The experimental data[47] are shown as solid line. Statistical uncertainties are smaller than the symbol size

The calculation of a binary vapor–liquid coexistence curve with a non-polar second compound is a good way to assess whether a newly developed force field for a polar compound possesses a good balance between dispersive and first-order electrostatic interactions[26,48]. The permanent dipole moments for different models are listed in Table II. All of the four-site models (Kristof et al.[12], Eckl et al.[28], and M-0) have dipole moments close to 1.9 D, i.e., about 30% higher than the experimental gas-phase dipole moment[48] but in line with the expectations from induced polarization for liquid ammonia[28]. For the models developed here, it is clear that an increase in the M-site displacement leads to a decrease in the dipole moment for the optimized model, and the dipole moment for model M-16 coincides with the experimental gas-phase value. Correspondingly, the Lennard–Jones well depth for the optimized models is found to increase with increasing M-site displacement (see Table I). Thus, the balance of dispersive and first-order electrostatic interactions shifts systematically for these models.

A projection of the binary phase diagram for ammonia + methane at $T$ = 273.15 K in the $P$–$x$ plane is shown in Fig. 3. The three models developed here are all able to reproduce the experimental data[50] reasonably well. The

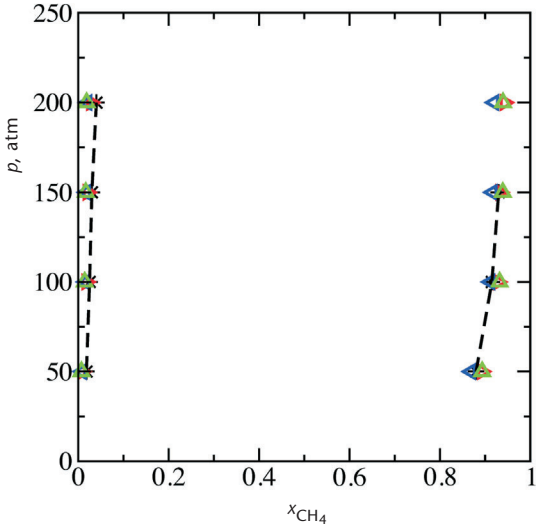


FIG. 3
Comparison of the $P$–$x$ diagram for the binary mixture of ammonia + methane predicted by different ammonia models. Symbols as in Fig. 1. The experimental data[50] are shown as stars and dashed line. Statistical uncertainties are smaller than the symbol size

mean unsigned errors in the composition (molfraction) are 0.010, 0.014, and 0.012 for models M-0, M-8, and M-16, respectively. Although these absolute errors are quite small, the relative error are much higher, but care must be taken because the relative error depends on whether it is computed for the minority or majority component in a given phase. All three models significantly underestimate (on average by factors of 1.6, 2.1, and 1.9, respectively) the methane molfraction in the ammonia-rich phase, whereas the molfraction of ammonia in the methane-rich phase is underestimated by factors of 1.1 and 1.2 for models M-0 and M-8, respectively, and overestimated by a factor of 1.1 for model M-16. The statistical uncertainties in the computation of the molfraction of the minority component are about 15 and 10% for the ammonia- and methane-rich phases; therefore the differences between the models are mostly within the uncertainties (and the error in the methane molfraction does not follow the order of the permanent dipole moments for the ammonia models). However, the underestimation of the methane molfraction by a factor close to 2 is significant. Nevertheless, this factor of 2 is in the acceptable range for solvation of a non-polar compound in a strongly polar compound when non-polarizable models are used. In fact, it is close to the change in the free energy of solvation that one can estimate for this case from the Born model for solvation in a continuum dielectric[51] and that have been computed from molecular simulations comparing polarizable and non-polarizable methane models in explicit water[52,53].

For non-polarizable models with similar geometry, the dielectric constant ($\varepsilon_D$) of a neat fluid phase is approximately proportional to the square of the permanent dipole moment ($\mu$) of the molecular model. Thus, the computation of the liquid-phase dielectric constant is also a good test to evaluate whether the ammonia models developed here give a good description of the first-order electrostatic interactions. Kristof et al.[12] already noted that their four-site model with $\mu$ = 1.90 D results in a large overestimation (by about 60%) of $\varepsilon_D$ for the liquid phase at 240 K, albeit the statistical uncertainty of their result is quite large (see Table II). Our model M-0 with the same geometry and permanent dipole moment yields a value of $\varepsilon_D = 37 \pm 4$ that is in good agreement with $\varepsilon_D$ for the model by Kristof et al.[12]. The liquid-phase dielectric constant was not calculated by Eckl et al.[28], but based on the dipole moment one may expect that their model would also significantly overestimate $\varepsilon_D$. Models M-8 and M-16 yield $\varepsilon_D$ values of $22 \pm 2$ and $12 \pm 1$, respectively. That is, the ratios are larger than what one would expect from $\mu^2$ but the geometry (placement of the charge sites) also

changes between these models. The prediction of $\varepsilon_D$ for model M-8 is in excellent agreement with the experimental value[48] of 22.4, whereas $\varepsilon_D$ for model M-16 is much too small. Thus, the computation of $\varepsilon_D$ strongly supports that model M-8 gives the best representation of the electrostatic interactions among the models evaluated here.

Traditionally, force fields have often been parameterized to reproduce structural information obtained from X-ray or neutron diffraction experiments. This is usually done by fitting to the partial radial distribution functions (RDFs) deduced from the experimental partial structure factors (PSFs). Although this procedure allows for visual comparison in real space and detailed structural information can be gleaned from partial RDFs, there are significant approximations and uncertainties in the conversion of a PSF to the corresponding RDF [54,55], and a more reliable approach would be the computation of the PSFs from the simulation trajectory. However, a quantitative mapping can only be made when the electronic densities are available from the simulations[54] which is not the case for force field based simulations. Thus, RDFs can only serve as a guide for the validation of the ammonia models developed here.

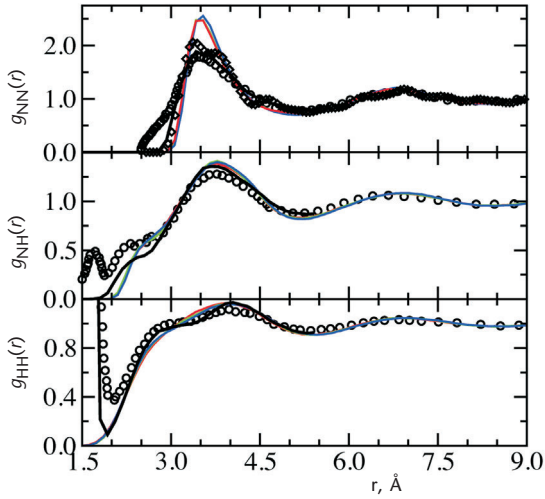


FIG. 4
Comparison of nitrogen–nitrogen (top), nitrogen–hydrogen (middle), and hydrogen–hydrogen (bottom) radial distribution functions near $T$ = 275 K. The circles and diamonds represent neutron[56] and X-ray[10] diffraction results, respectively. The black, red, green, and blue lines depict the data from first principles simulations[57] and for models M-0, M-8, and M-16, respectively

Figure 4 shows a comparison of the partial RDFs obtained for the three models developed here to those deduced from the X-ray diffraction experiments by Narten[10] and the neutron diffraction experiments by Ricci et al.[56]. The most important observation from the RDFs is the extremely close agreement found among the three models. Given this close agreement, the partial RDFs are obviously not well suited to select between models M-0, M-8, and M-16. Furthermore, these partial RDFs are also in very close agreement with those obtained by Kristof et al.[12] and Eckl et al.[28]. Although it appears at first hand that the partial RDFs are lacking many of the structural features of the experimentally deduced RDFs, many of them are either due to intramolecular features (the peak at $r$ = 1.6 Å in the hydrogen–hydrogen RDF), due to H/D exchange effects (the peak at $r$ = 1.7 Å in the nitrogen–hydrogen RDF), or believed to be artifacts of the data treatment (the shoulder at $r$ = 3.8 Å in the nitrogen–nitrogen RDF). An excellent discussion of the structural features of liquid ammonia together with PSFs and RDFs obtained from first principles molecular dynamics simulations has been given by Diraison et al.[57]. For the present work, it is important to note that the partial RDFs obtained for the empirical force fields are much closer to those from the first principles simulations than the experimentally deduced RDFs. Nevertheless, it is clear that models M-0, M-8, and M-16 slightly overestimate the height of the first peak in the nitrogen–nitrogen RDF and slightly underestimate the hydrogen-bonding shoulder ($r \approx 2.4$ Å) in the nitrogen–hydrogen RDF.

## CONCLUSIONS

With the aim to develop a rigid non-polarizable ammonia model for the TraPPE force field, this work explored the parameterization of three five-site models with a single Lennard–Jones site at the position of the nitrogen atom and 4 partial charges placed at the location of the hydrogen atoms and an additional M site. Three different displacements of the M site were investigated. Model M-8 with an intermediate displacement of the M site is found to perform slightly better for the vapor–liquid equilibrium properties of neat ammonia and significantly better for the liquid-phase dielectric constant than the other two models. In contrast, neither the calculation of the binary vapor–liquid coexistence curve with methane nor the partial radial distribution functions show a significant difference between the three models. Thus, model M-8 is selected for incorporation as non-polarizable model into the TraPPE force field. The ongoing development of polarizable force field[58] may lead to a better description for mixtures of polar and non-

polar compounds but will also lead to a substantial increase in the computational cost.

*Financial support from the National Science Foundation (CBET-0553911 and CBET-0756641) is gratefully acknowledged. Part of the computer resources was provided by the Minnesota Supercomputing Institute.*

**REFERENCES**

1. Kolafa J., Nezbeda I.: *Mol. Phys.* **1991**, *72*, 777.
2. Predota M., Nezbeda I., Kalyuzhnyi Y. V.: *Mol. Phys.* **1998**, *94*, 937.
3. Vlček L., Nezbeda I.: *Mol. Phys.* **2004**, *102*, 485.
4. Vlček L., Nezbeda I.: *Mol. Phys.* **2004**, *102*, 771.
5. Jirsák J., Nezbeda I.: *J. Mol. Liq.* **2007**, *134*, 99.
6. Jorgensen W. L., Ibrahim M.: *J. Am. Chem. Soc.* **1980**, *102*, 3309.
7. Hinchliffe A., Bounds D. G., Klein, M. L., McDonald I. R., Righini R.: *J. Chem. Phys.* **1981**, *74*, 1211.
8. Impey R. W., Klein M. L.: *Chem. Phys. Lett.* **1984**, *104*, 579.
9. Benedict W. S., Plyler E. K.: *Can. J. Phys.* **1985**, *35*, 890.
10. Narten A. H.: *J. Chem. Phys.* **1977**, *66*, 3117.
11. Rizzo R. C., Jorgensen, W. L.: *J. Am. Chem. Soc.* **1999**, *121*, 4827.
12. Kristof T., Vorholz J., Liszi J., Rumpf B., Maurer G.: *Mol. Phys.* **1999**, *97*, 1129.
13. Zhang L.: *Ph.D. Thesis*. University of Minnesota, Minneapolis 2006.
14. Martin M. G., Siepmann J. I.: *J. Phys. Chem. B* **1998**, *102*, 2569.
15. Martin M. G., Siepmann J. I.: *J. Phys. Chem. B* **1999**, *103*, 4508.
16. Chen B., Siepmann J. I.: *J. Phys. Chem. B* **1999**, *103*, 5370.
17. Nath S. K., Escobedo F. A., de Pablo J. J.: *J. Chem. Phys.* **1998**, *108*, 9905.
18. Errington J. R., Panagiotopoulos A. Z.: *J. Phys. Chem. B* **1999**, *103*, 6314.
19. Ungerer P., Beauvais C., Delhommelle J., Boutin A., Rousseau B., Fuchs A. H.: *J. Chem. Phys.* **2000**, *112*, 5499.
20. Bourasseau E., Haboudou M., Boutin A., Fuchs A. H., Ungerer P.: *J. Chem. Phys.* **2003**, *118*, 3020.
21. Chen B., Potoff J. J., Siepmann J. I.: *J. Phys. Chem. B* **2001**, *105*, 3093.
22. Stubbs J. M., Potoff J. J., Siepmann J. I.: *J. Phys. Chem. B* **2004**, *108*, 17596.
23. Wick C. D., Stubbs J. M., Rai N., Siepmann J. I.: *J. Phys. Chem. B* **2005**, *109*, 18974.
24. Lubna N., Kamath G., Potoff J. J., Rai N., Siepmann J. I.: *J. Phys. Chem. B* **2005**, *109*, 24100.
25. Perez-Pellitero J., Bourasseau E., Demachy I., Ridard J., Ungerer P., Mackie A. D.: *J. Phys. Chem. B* **2008**, *112*, 9853.
26. Potoff J. J., Siepmann J. I.: *AIChE J.* **2001**, *47*, 1676.
27. Rai N., Siepmann J. I.: *J. Phys. Chem. B* **2007**, *111*, 10790.
28. Eckl B., Vrabec J., Hasse H.: *Mol. Phys.* **2008**, *106*, 1039.
29. Maitland G. C., Rigby M., Smith E. B., Wakeham A.: *Intermolecular Forces: Their Origin and Determination*. Pergamon, Oxford 1987.
30. Wood W. W., Parker F. R.: *J. Chem. Phys.* **1957**, *27*, 720.

31. Allen M. P., Tildesley D. J.: *Computer Simulations of Liquids*. Oxford, Oxford 1987.
32. Panagiotopoulos A. Z.: *Mol. Phys.* **1987**, *61*, 813.
33. Panagiotopoulos A. Z., Quirke N., Stapleton M., Tildesley D. J.: *Mol. Phys.* **1988**, *63*, 527.
34. Siepmann J. I., Frenkel D.: *Mol. Phys.* **1992**, *75*, 59.
35. Mooij G. C. A. M., Frenkel D., Smit B.: *J. Phys.: Condens. Matter* **1992**, *4*, L255.
36. Laso M., de Pablo J. J., Suter U. W.: *J. Chem. Phys.* **1992**, *97*, 2817.
37. Vlugt T. J. H., Martin M. G., Smit B., Siepmann J. I., Krishna R.: *Mol. Phys.* **1998**, *94*, 727.
38. Rowlinson J. S., Widom B.: *Molecular Theory of Capillarity*. Oxford, New York 1989.
39. Rowlinson J. S., Swinton F. L.: *Liquids and Liquid Mixtures*. Butterworth, London 1982.
40. Leguillou J. C., Zinn-Justin J.: *Phys. Rev. B* **1980**, *21*, 3976.
41. Antoine C.: *C. R. Acad. Sci.* **1888**, *107*, 681.
42. Atkins P. W.: *Physical Chemistry*. Oxford University, New York 2002.
43. McDonald I. R.: *Mol. Phys.* **1972**, *23*, 41.
44. Chen B., Potoff J. J., Siepmann J. I.: *J. Phys. Chem. B* **2000**, *104*, 2378.
45. Bender E.: *Proc. Symp. Thermophys. Prop.* **1970**, *5*, 227.
46. Mathews J. F.: *Chem. Rev.* **1972**, *72*, 71.
47. Lide D. R: *CRC Handbook of Chemistry and Physics*, 86th ed. CRC, Cleveland 2005.
48. Wick C. D., Siepmann J. I., Klotz W. L., Schure M. R.: *J. Chromatogr., A* **2002**, *954*, 181.
49. Rai N., Siepmann J. I.: *J. Phys. Chem. B* **2007**, *111*, 10790.
50. Nohka J., Sarashina E., Arai Y., Saito S.: *J. Chem. Eng. Jpn.* **1973**, *6*, 10.
51. Cramer C. J.: *Essentials of Computational Chemistry: Theories and Models*. Wiley, Chichester 2004.
52. Chen B.: *Ph.D. Thesis*. University of Minnesota, Minneapolis 2001.
53. Dyer P. J., Docherty H., Cummings P. T.: *J. Chem. Phys.* **2008**, *129*, 024508.
54. Hura G., Russo D., Glaeser R. M., Head-Gordon T., Krack M., Parrinello M.: *Phys. Chem. Chem. Phys.* **2003**, *5*, 1981.
55. Soper A. K.: *J. Phys.: Condens. Matter* **2007**, *19*, 415108.
56. Ricci M. A., Nardone M., Ricci F. P., Andreani C., Soper A. K.: *J. Chem. Phys.* **1995**, *102*, 7650.
57. Diraison M., Martyna G. J., Tuckerman M. E.: *J. Chem. Phys.* **1999**, *111*, 1096.
58. Chen B., Xing J., Siepmann J. I.: *J. Phys. Chem. B* **2000**, *104*, 2391.